applied sciences

MDPI

Article

Study on Relay Contact Bounce Based on the Adaptive Weight Rotation Template Matching Algorithm

Wenze Zhao [1], Jiaxing Yan [1], Xin Wang [2], Wenhua Li [1,*], Xinglin Yang [1] and Weiming Wang [1]

[1] State Key Laboratory of Reliability and Intelligence of Electrical Equipment, Hebei University of Technology, Tianjin 300401, China
[2] Shenyang Railway Signal Co., Ltd., Shenyang 110025, China
* Correspondence: liwenhua@hebut.edu.cn

Abstract: In order to analyze the relay action process from an imaging perspective and further investigate the bounce phenomenon of relay contacts during the contact process, this paper utilizes a high-speed shooting platform to capture images of relay action. In light of the situation where the stationary contact in the image is inclined and continuously changing, a rotation template matching algorithm based on adaptive weight is proposed. The algorithm identifies and obtains the inclination angle of the stationary contact, enabling the study of the relay contact bounce process. By extracting contact bounce distance data from the images, a bounce process curve is plotted. Combined with the analysis of the contact bounce process, the reasons for the bounce are explored. The results indicate that the proposed rotation template matching algorithm can accurately identify stationary contacts and their angles at different angles. By analyzing the contact status and bounce process of the relay contacts in conjunction with the relay structure, parameters such as the bounce time, bounce height, and time required to reach the maximum distance can be calculated. Additionally, the main reason for contact bounce in the relay studied in this paper is the limitation imposed on the continued movement of the stationary contact by the presence of the relay brackets when the kinetic energy of the contact is too high. This phenomenon occurs during the first vibration peak in the vibration process after the moving contact contacts the stationary contact. The research results provide a reference for further studying the relay contact bounce process, optimizing relay structure, and suppressing contact bounce.

Keywords: relay; contact bounce; adaptive weight; rotational template matching; image processing

Citation: Zhao, W.; Yan, J.; Wang, X.; Li, W.; Yang, X.; Wang, W. Study on Relay Contact Bounce Based on the Adaptive Weight Rotation Template Matching Algorithm. *Appl. Sci.* **2024**, *14*, 2341. https://doi.org/10.3390/app14062341

Academic Editor: Andreas Sumper

Received: 1 February 2024
Revised: 4 March 2024
Accepted: 7 March 2024
Published: 11 March 2024

1. Introduction

Relays are electrical control components with isolation functionality, capable of controlling large currents or voltages through small currents or voltages. They offer advantages such as a high switching capacity, excellent isolation performance, fast response, and ease of control and use [1]. The moving contact and the stationary contact, serving as critical components for signal switching in relays, may experience the phenomenon of contact bounce during their contact process. This occurrence not only leads to transient instability in the relay's output signal during the switching process, affecting the normal operation of controlled circuits or devices, but also accelerates wear and oxidation on the contact surfaces due to repeated collisions and friction, significantly impacting the contact's lifespan and reliability. Therefore, the study of relay contact bounce is an essential aspect of relay analysis.

For all kinds of switching appliances, contact bounce phenomenon research started early. Since as early as the 20th century, there have been a lot of studies on the contact bounce phenomenon for tests, research, and analyses of its influence factors [2–5]. In recent years, with the continuous development and progress of science and technology, the means of research on contact bouncing have gradually increased. Zhai et al. [6–9] analyzed contact

bounce characteristics and behavior by building a kinetic model of the contact bounce of a relay, contactor, and other switching appliances and adopting the method of multi-physics field simulation and calculations. Ren et al. [10–12] studied the contact bounce of a relay by building an experimental device and testing the related parameters. Xu et al. [13–15] proposed a new approach to the contact bounce of an AC relay from the perspective of optimizing the system structure and the control process; they proposed a suppression strategy for AC contactor bounce. Huang et al. [16–18] analyzed the contactor bounce behavior law by ADAMS simulation and optimized it with an algorithm. Fabian Winkel et al. [19] also proposed a bounce optimization algorithm to reduce contact bounce by optimizing the control signal.

However, current research on contact bounce primarily relies on simulation analysis, often complemented by voltage data collection and displacement sensors for validation. It remains challenging to accurately grasp the true motion of contacts throughout the entire process. Additionally, voltage data collection is limited in its ability to analyze the bounce distance during the rebound process, as it can only calculate bounce time. The application scope of displacement sensors is somewhat restricted, making accurate measurements difficult in certain situations.

Machine vision technology, utilizing high-speed cameras to capture images and combining them with image processing techniques, offers a comprehensive analysis of various aspects such as time and distance. In recent years, it has gradually become one of the mainstream methods in relay research [20–22].

Therefore, the main objective of this paper is to utilize machine vision technology to capture and recognize images of cylindrical contact points in relays. Through image processing, the aim is to obtain the positions and angles of the contact points. Subsequently, by quantifying the bounce phenomenon based on the separation distance between the contacts, the paper seeks to analyze the relay's contact bounce phenomenon and its related parameters to optimize the structure of the relay.

To achieve this goal, this paper proposes an adaptive weight rotation template matching algorithm. This algorithm can better handle changes in target angles and identify targets at different angles after rotation. Furthermore, applying this algorithm to the study of bounce phenomena in cylindrical contact relays differs from existing methods, which can only indirectly calculate the contact bounce time through voltage data. This method allows for a more direct observation of the entire bounce process of relay contacts and the acquisition of the distance curve between the moving and stationary contacts. Parameters such as the bounce time, bounce height, and time required to reach the maximum rebound distance can be calculated. Additionally, by combining image and data analyses to understand the causes of bounce, this paper provides a reference for guiding improvements in relay products and suppressing contact bounce.

2. Introduction to the Research Subjects

The relay studied in this paper is a heavy, elastic, DC, magnetic-type electrodeless relay of a DC 24V series. The contacts of the relay are typical cylindrical contacts. To analyze the process of relay contact bounce through imaging, a high-speed camera was used to capture images of the contact motion during the relay action. The high-speed camera is a Pco.dimax S model high-speed camera developed by KUK, Bad Schönborn, Germany, and the optical lens is an AF-S VR Micro-Nikkor 105 mm f/2.8 G IF-ED from Nikon (Tokyo, Japan). Some of the key parameters of the camera and the optical lens are shown in Tables 1 and 2, respectively. The set camera acquisition frequency is 10,000 frames/s, and the acquired relay images are shown in Figure 1.

Table 1. Key parameters of high-speed camera.

Parameter Name	Parameter Size
Maximum resolution	1008 × 1008
Maximum frame rate	152,811 fps
Exposure time	1.5 μs–40 ms

Table 2. Key parameters of optical lens.

Parameter Name	Parameter Size
Focal length	105 mm
Aperture	f/2.8–f/32
Magnification rate	1:1–1:10

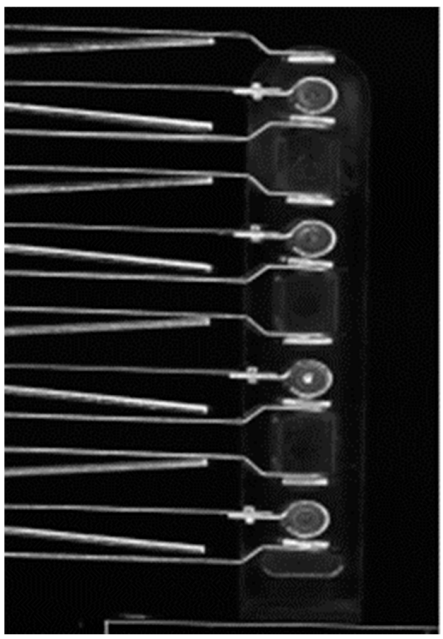

Figure 1. Relay image acquired by high-speed camera.

The bounce of relay contacts refers to the phenomenon where the contacts of a relay close and open multiple times in a short period due to mechanical vibrations or the elasticity of the springs during the closing process [23]. In the contact bounce process, the bounce time refers to the duration during which the relay experiences an intermittent disconnection of contacts when closing or an intermittent closure of contacts when opening [24]. The bounce height is the maximum distance over which the contacts open during the contact bounce period [25]. The time required to reach the maximum distance is the duration from the moment the contacts begin to separate until the contacts reach their maximum separation distance.

For the relay studied in this paper, its structural components are illustrated in Figure 2. When the relay contacts close or open, under the influence of electromagnetic force or gravity, the moving contact and the stationary contact come into contact and move together for a certain distance, exceeding their stable positions. This causes a certain amount of elastic deformation in the reed. When the elastic force generated by the deformation exceeds the electromagnetic force or gravity, it leads to a rebound of the contacts. In this process, the moving contact and the stationary contact vibrate together, and contact bounce typically occurs during this stage.

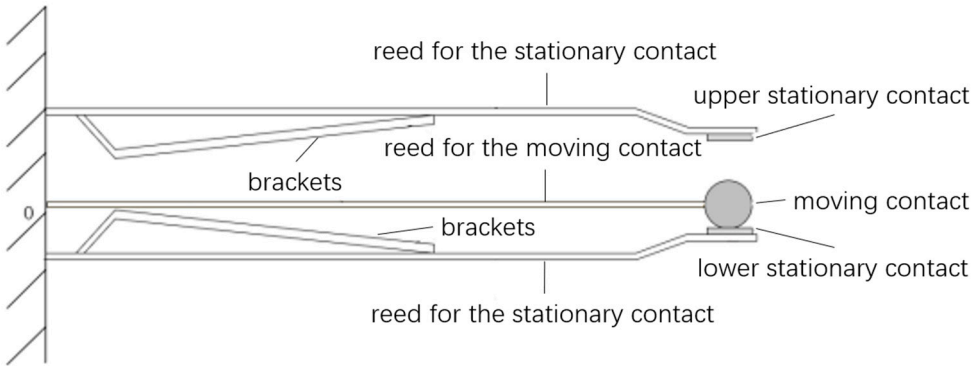

Figure 2. Schematic diagram of the structure of each part of the relay.

The partial sequence images of a single set of contacts during the relay action process are depicted in Figure 3. Combining these images with the relay's action process, it is evident that the side view of the stationary contact during the relay's action process forms an inclined rectangle. As the relay contacts undergo actions such as attraction and release, the inclination angle of the stationary contact changes accordingly. Calculating the relay contact bounce requires analyzing the position and angle of the stationary contact in the side view image. Therefore, an appropriate recognition algorithm is needed that can accurately select the position and edges of the stationary contact while obtaining its inclination angle.

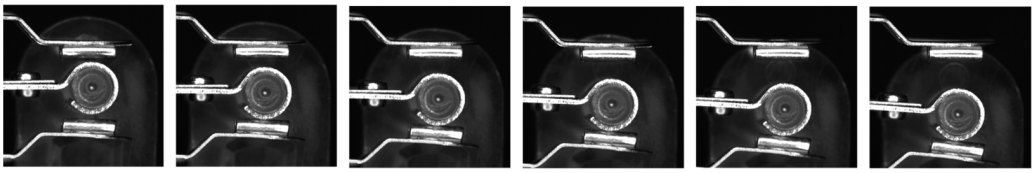

Figure 3. Partial image sequence of relay contact action process.

3. Adaptive Weight Rotation Template Matching Algorithm

3.1. Basic Flow of Rotating Template Matching Algorithm

To achieve accurate identification of the stationary contact, this paper proposes a rotation template matching algorithm with adaptive weight. The basic process of the algorithm is illustrated in Figure 4. Firstly, capture a template image of a stationary contact point. Set the minimum angle for template rotation, θ_{min}, and maximum angle, θ_{max}, as well as the angle step size for each rotation, θ_{step}. Rotate the template from the minimum angle, θ_{min}, and when it starts rotating, the rotation angle increases each time, θ_{step}, until the rotation angle increases to θ_{max}. This generates a series of rotation templates at different angles. Then, match these templates individually with the relay image. The position and edges of the stationary contact in the image correspond to the highest matching position of the template, and the rotation angle of this template indicates the inclination angle of the stationary contact at that moment.

3.2. Principle of Template Matching Algorithm

The template matching algorithm serves as the core algorithm, with the fundamental concept being to slide a fixed-size template across the image to be matched, calculate the similarity between the template and the local region of the image, and identify the position with the highest similarity as the matching result.

For the target stationary contact in the relay image, its feature points and shape contour are not obvious, especially in the process of relay action where the contact angle changes. The feature points and shape may also change. Choosing the two methods based on feature descriptors and shape-based matching is prone to matching inaccuracy in such a situation. Therefore, we opt for the most traditional method based on pixel comparison for matching.

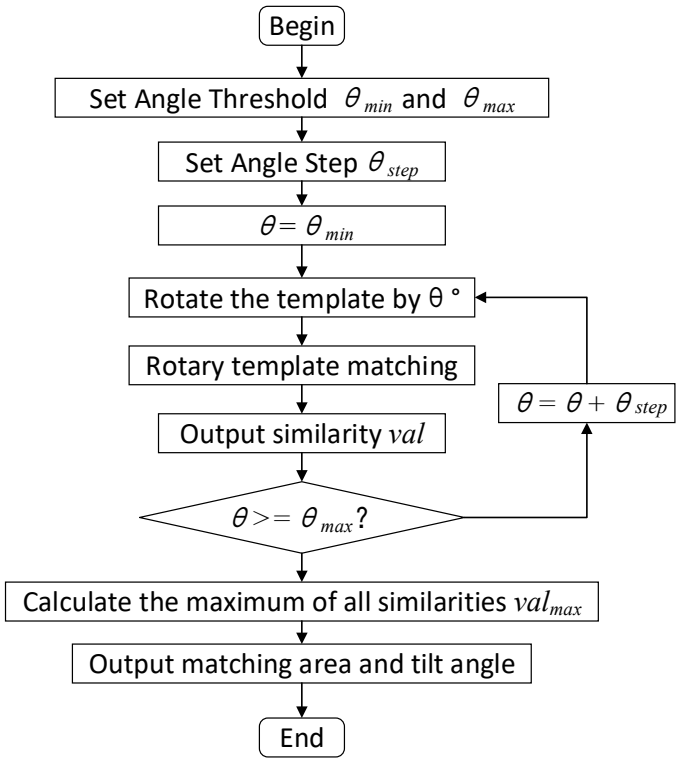

Figure 4. Flowchart of the rotating template matching algorithm.

First, set a sliding window with a size equal to the template size. Apply the sliding window to the image to be matched, starting from the upper-left corner of the image. Move along the horizontal and vertical directions of the image with a certain step size to find the matching position. For each sliding window position, compare the image region in the window pixel by pixel with the template and calculate the similarity between them.

Zero-mean Normalized Cross-Correlation (ZNCC) is a commonly used similarity metric which calculates the number of correlations between the template and the image regions to be matched and normalizes them, and the number of correlations reflects the linear relationship between them [26]. The specific calculation method is as follows: Firstly, the template image and the target image are de-meaned, and then the pixel values in the corresponding positions of the de-meaned template region and the image region are multiplied. Then, all the product values are summed up, and the variance of the pixel values in the de-meaned image region and the template region is calculated, and the product and the variance are normalized.

With I representing the image to be matched and T representing the template image, let $I(x,y)$ and $T(x,y)$ denote the pixel values of the target image and the template image at position (x,y), respectively. The formula for the normalized inter-correlation method is as follows:

$$NCC = \frac{\sum_{x=0}^{m-1}\sum_{y=0}^{n-1}[(T(x,y)-\mu T)\times(I(x,y)-\mu I)]}{\sqrt{\sum_{x=0}^{m-1}\sum_{y=0}^{n-1}[(T(x,y)-\mu T)]^2 \times \sum_{x=0}^{m-1}\sum_{y=0}^{n-1}[(I(x,y)-\mu I)]^2}} \quad (1)$$

where m and n denote the size of the template image and the target image, respectively, and μI and μT represent the pixel mean value of the image region and the template region, respectively, calculated as follows:

$$\mu T = \frac{1}{m \times n} \sum_{x=0}^{m-1} \sum_{y=0}^{n-1} T(x, y) \tag{2}$$

$$\mu I = \frac{1}{m \times n} \sum_{x=0}^{m-1} \sum_{y=0}^{n-1} I(x, y) \tag{3}$$

3.3. Template Image Rotatation

After determining the similarity measurement method, use the center rotation method to achieve image rotation and obtain the rotated template image. The center rotation of an image is similar to the rotation of a point in a Cartesian coordinate system, as illustrated in Figure 5, where point P is rotated around the origin O as the rotation center to obtain point Q.

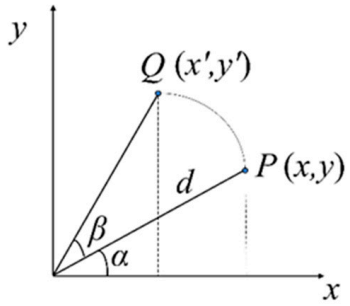

Figure 5. Schematic diagram of the rotation of a point in space.

Let the distance from point P to the origin be d, i.e., the rotation radius is d. The coordinates of point Q, (x', y'), can be obtained using trigonometry as follows:

$$\begin{cases} x' = d \times \cos(\alpha + \beta) \\ y' = d \times \sin(\alpha + \beta) \end{cases} \tag{4}$$

Simplifying the above equation yields the result shown in the following equation:

$$\begin{cases} x' = \cos \beta x - \sin \beta y \\ y' = \sin \beta x + \cos \beta y \end{cases} \tag{5}$$

Taking the geometric center of the image as the center of rotation rotates the image around the center of rotation, with the principle of rotation being the same as that of a point, as illustrated in Figure 6.

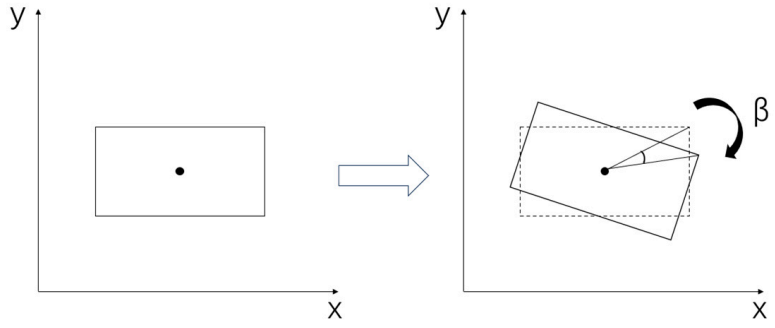

Figure 6. Schematic diagram of image center rotation.

Since the tilted image after rotation will be out of the range of the original image size, the generated image template will remain a horizontal rectangle. A panning search during template matching is also conducted using a horizontal, rectangular window. There are two ways of generating an image to choose from:

(1) The size of the generated image remains the same as the original image, but local loss of the original image occurs after rotation, as illustrated in Figure 7a. The red rectangle in the figure represents the original image after rotation, and the dashed box rectangle represents the original image before rotation and the size of the new image generated after rotation. The blue area in the figure is the filled area, and the red area outside the dashed line is the missing original image area.

(2) After rotation, the original image size remains unchanged, while the newly generated image is larger than the original image size, as illustrated in Figure 7b. The red rectangle in the figure represents the original image after rotation, the dashed box rectangle represents the original image before rotation, the blue rectangle represents the size of the new image generated after rotation, and the blue area in the figure is the filled area.

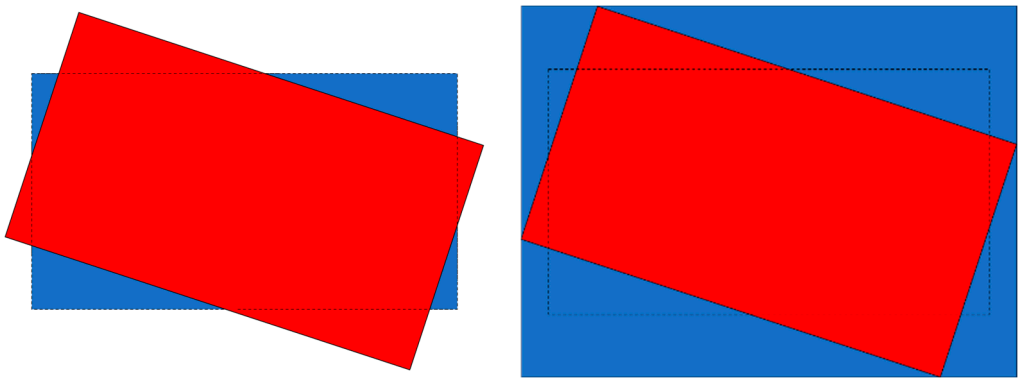

(**a**) (**b**)

Figure 7. Schematic diagram of the template image generated after rotation: (**a**) the size of the image generated after rotation remains the same; (**b**) the size of the image generated after rotation changes.

The first case will affect the overall size and shape of the actual matched template, and the changes under different angles are different, with no guaranteed accuracy in the match. On the other hand, the second case changes the overall size of the image, but the size and shape of the original image remain unchanged, not affecting the actual matching effect. Therefore, the second rotational method is used to generate the image. The captured stationary contact template image is shown in Figure 8a, and the template image generated by rotating it is shown in Figure 8b. In Figure 8b, the tilted image in the middle is the original template image after rotation, corresponding to the red rectangle in Figure 7b. The blue area at the four corners of the image is the vacant area generated in the rotated image, which is filled in black by default. For ease of observation, this article uses blue for filling, which corresponds to the blue area in Figure 7b. If the template matching algorithm is directly used for matching according to this image, regardless of the pixel value filled in the blank area, the filled pixel value will also participate in the calculation of the matching result. Even if the vacant area's pixel value is zero, it will affect the final calculation results, leading to inaccurate matching results and affecting the recognition effect. Therefore, the similarity measure formula in the template matching algorithm needs improvement to eliminate the influence of the vacant region.

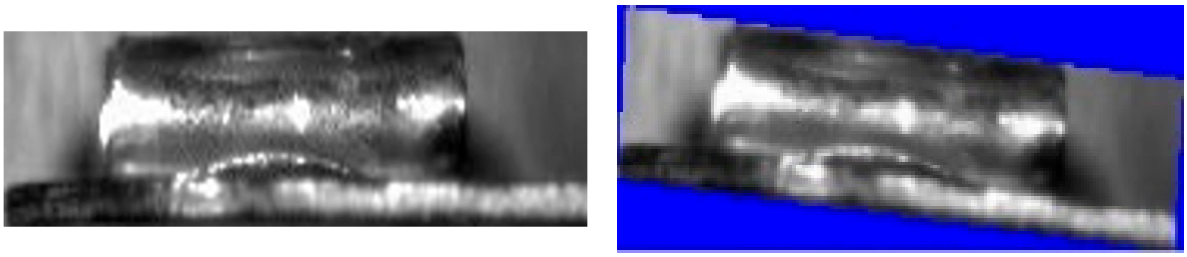

(**a**) (**b**)

Figure 8. Comparison of templates before and after rotation: (**a**) the template image before rotation; (**b**) the template image generated after rotation.

3.4. Improvement of Similarity Formula Based on Adaptive Weight

To address the above situation, the paper proposes improving the similarity metric formula using the method of adaptive weight, as illustrated in Figure 9. Assuming that the size of the original template is H*W and the rotation angle is θ, the size of the new template generated can be calculated with the trigonometric formula, and its width and height are, respectively:

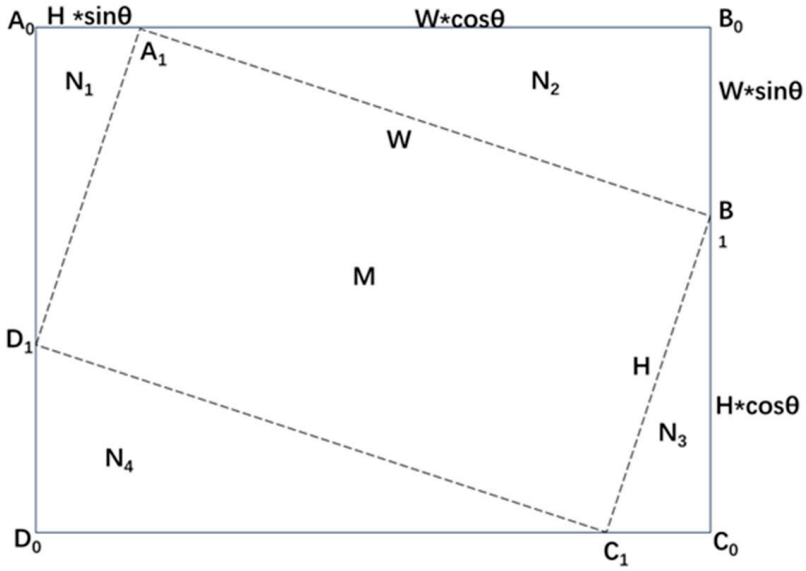

Figure 9. Schematic diagram of weight matrix generation.

$$W' = H * \sin\theta + W * \cos\theta \tag{6}$$

$$H' = W * \sin\theta + H * \cos\theta \tag{7}$$

Simultaneously with the generation of rotated templates, an adaptive weight matrix, ω, corresponding to each template is dynamically generated. This means that based on the size of the template image and the angle of rotation, the weight matrix corresponding to the template at a specific rotation angle is adaptively constructed. This weight matrix is crucial for calculating the similarity between the template and the target image during the template matching process. The size of the matrix is the same as the size of the template, and the elements within the matrix are 0 and 1. The matrix elements within the original image region M (the rectangular dashed box region in the figure) are all 1 after rotation, and the matrix elements within the filled regions N_1, N_2, N_3, and N_4 (the region between the rectangular dashed box and the rectangular solid box in the figure) outside of the original image after rotation are all 0. Next, the similarity formula needs to be updated by incorporating the rotated template.

First, the weight matrix is used to recalculate the mean values of the images to be matched and the template image. Only the mean value of the region corresponding to the original template in the rotated template image needs to be calculated. This means calculating the mean value of the matrix elements in the images to be matched and the template image corresponding to the positions where the elements of the weight matrix are 1. The corresponding calculation formulas are as follows:

$$\mu \mathrm{T}' = \frac{\sum_{\mathrm{x}=0}^{m-1} \sum_{y=0}^{n-1} T(x,y) \times \omega(x,y)}{m \times n - \mathrm{n}_0} \tag{8}$$

$$\mu \mathrm{I}' = \frac{\sum_{\mathrm{x}=0}^{m-1} \sum_{y=0}^{n-1} I(x,y) \times \omega(x,y)}{m \times n - \mathrm{n}_0} \tag{9}$$

where m is the number of rows in the matrix, n is the number of columns in the matrix, (i,j) denotes the element in the i-th row and j-th column of the matrix, and n_0 denotes the number of 0 elements in the weight matrix.

Then, it is necessary to calculate the inner product of the two matrices after de-meaning. In calculating the inner product, again, only the inner products of the elements in the target region of the matrix need to be calculated, and the improved formula for calculating the inner product is as follows:

$$\sum_{x=0}^{m-1} \sum_{y=0}^{n-1} [(T(x,y) - \mu T') \times (I(x,y) - \mu I') \times \omega] \tag{10}$$

When performing the normalization calculation, the product of the sum of the squares of the two matrices after calculating the demeaned value also needs to be removed from the non-target region, and the improved formula for calculating the sum of the squares of the matrices is as follows:

$$\sum_{x=0}^{m-1} \sum_{y=0}^{n-1} [(T(x,y) - \mu T') \times \omega]^2 \times \sum_{x=0}^{m-1} \sum_{y=0}^{n-1} [(I(x,y) - \mu I') \times \omega]^2 \tag{11}$$

Combining the above equations results in the following formula for calculating the similarity in the final rotating template matching algorithm:

$$NCC' = \frac{\sum_{x=0}^{m-1} \sum_{y=0}^{n-1} [(T(x,y) - \mu T') \times (I(x,y) - \mu I') \times \omega]}{\sqrt{\sum_{x=0}^{m-1} \sum_{y=0}^{n-1} [(T(x,y) - \mu T') \times \omega]^2 \times \sum_{x=0}^{m-1} \sum_{y=0}^{n-1} [(I(x,y) - \mu I') \times \omega]^2}} \tag{12}$$

By calculating with the improved formula, the influence of the rotated vacant area on the calculation results can be eliminated, avoiding interference and ensuring the accuracy of the recognition.

3.5. Finalization of Results

Traverse the generated template through a sliding window through the image, and calculate the similarity of the template in each region of the image using the similarity formula mentioned earlier. The maximum value of the template's corresponding similarity is the template's matching similarity, and the coordinates of the region corresponding to the maximum similarity are the matching coordinates. Calculate the matching similarity, $val_{\theta i}$,

of the templates in the image for each angle, θ_i, using the same method, and summarize them to obtain a similarity matrix:

$$Vals = [val_{\theta 1}, val_{\theta 2}, \ldots, val_{\theta i}, \ldots] \tag{13}$$

Calculate the maximum value of similarity, val_{max}, in the similarity matrix. The template corresponding to this similarity is the target template, and the matching coordinates of this template are the target region matched by the template. The rotation angle corresponding to this template is the tilt angle of the contact obtained. However, the size of this target region is the overall size of the image corresponding to the new template generated after the rotation, as shown in the blue rectangular box in the figure. In order to obtain the corresponding contact edges completely, we need to restore the original template region from the region after the rotation.

The method of restoration can be realized by calculating the vertices, as shown in the figure. Assuming that the coordinates of the lower left vertex, D_0, of the matching region corresponding to the new template are (x_0,y_0), the coordinates of the four vertices of the original template after the rotation, A_1, B_1, C_1, and D_1, can be calculated as follows:

$$\begin{cases} x_1 = x_0 + H * \sin\theta \\ y_1 = y_0 + W * \sin\theta + H * \cos\theta \end{cases} \tag{14}$$

$$\begin{cases} x_2 = x_0 + H * \sin\theta + W * \cos\theta \\ y_2 = y_0 + H * \cos\theta \end{cases} \tag{15}$$

$$\begin{cases} x_3 = x_0 + W * \cos\theta \\ y_3 = y_0 \end{cases} \tag{16}$$

$$\begin{cases} x_4 = x_0 \\ y_4 = y_0 + W * \sin\theta \end{cases} \tag{17}$$

By connecting the four vertices A_1, B_1, C_1, and D_1 in turn, the final matched target region can be obtained. As shown in the red dashed rectangular box in Figure 10, the connecting line of the four vertices forms the edge of the target stationary contact.

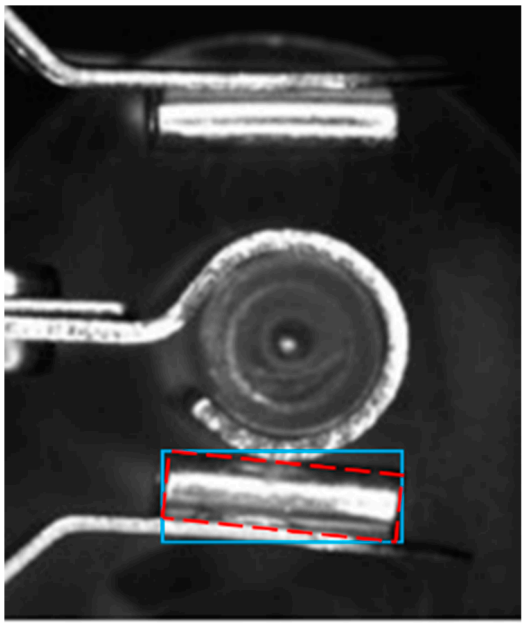

Figure 10. Schematic of target framing after rotation.

In the actual recognition process, it is necessary to set the angle range and step size of the generated rotary template. The angle range relates to the accuracy and speed of recognition, while the angle step size is crucial for accuracy and speed. Too large a range or too small a step can enhance recognition accuracy, but it will lead to too many templates and a significant decrease in recognition speed. If the range is too small, it will not cover all the angles of the contact, rendering recognition impossible. If the step is too large, it will affect recognition accuracy and increase recognition errors. To enhance recognition speed while maintaining the algorithm's accuracy, employing multi-threading in parallel could be considered. Each target angle could be assigned a separate thread for recognition. This approach enables simultaneous recognition of multiple angles, followed by result aggregation for comparison and analysis to accomplish recognition. Additionally, adopting an image pyramid can expedite algorithm processing. Initially, recognition can be performed on the top-level, low-resolution image of the pyramid, followed by recognition around the target position in the next lower level, until recognition is completed in the original image at the bottom level.

After several tests for the relay studied in this paper, the angle range of the stationary contact rotation template was set between -10° and 5°, and the step size of the rotation angle was 0.1°. This can cover all the tilt angles of the stationary contact during the action process, ensuring recognition accuracy and also improving recognition speed as much as possible. The adaptive rotary template matching algorithm is used to recognize the relay part of the image sequence, and the recognition results are shown in Figure 11.

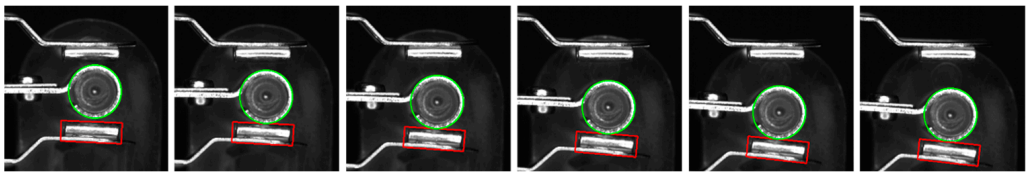

Figure 11. Effect of identifying relay stationary contacts at different angles.

To validate the algorithm's recognition performance, both the traditional normalized cross-correlation method (Equation (1)) and the improved formula (Equation (13)) were separately utilized as similarity calculation formulas for the rotation template matching algorithm. These were then compared with the traditional template matching algorithm. A set of complete images from the relay's operational process were selected for testing, with IoU (Intersection over Union) used as the accuracy evaluation metric. IoU represents the ratio of the intersection area between the predicted bounding box and the ground truth bounding box to the union area. The calculation formula is as follows:

$$IoU = \frac{Intersection}{Union} \tag{18}$$

where "*Intersection*" represents the area of overlap between the detection box and the ground truth box, while "*Union*" represents the area of union between the detection box and the ground truth box.

When IoU is greater than 0.9, it is considered a successful match. Using this criterion, we can calculate the recognition accuracy of each algorithm. The calculation formula is as follows:

$$Accuracy = \frac{TP + TN}{TP + TN + FP + FN} \tag{19}$$

where TP represents true positives, TN represents true negatives, FP represents false positives, and FN represents false negatives.

The final test results are shown in Table 3. It can be observed from the table that the accuracy of the rotation template matching algorithm, after the improvement of the similarity calculation formula, can reach over 98%. This represents a significant improvement

in accuracy compared to both traditional template matching algorithms and traditional formula-based template matching algorithms.

Table 3. Comparison of the effectiveness of different template matching algorithms.

Algorithm	Accuracy
Traditional template matching algorithm	54.3%
The rotation template matching algorithm for traditional formulas	71.9%
Improved formula-based rotation template matching algorithm	98.7%

4. Contact Bounce Analysis

4.1. Analysis of Contact Bounce Process

In this paper, viewed through the lens of image processing and taking into account the characteristics of the tested relay, the contact bounce is redefined: when the relay absorbs or releases the contact, in the process of the joint vibration of the relay contacts, if the movable contact and the corresponding stationary contact are separated, it is considered that a contact bounce has occurred.

Therefore, the critical aspect of analyzing contact bounce is determining the contact state of the moving contact and the stationary contact. As the moving contact appears as a circle and the stationary contact as a rectangle in the image, the contact problem of the moving contact and the stationary contact can be transformed into the tangent problem of the circle and the rectangle, as shown in Figure 12. Through the Hough circle detection algorithm, the coordinates of the center of the circle, (x_0,y_0), and the radius size, r, of the moving contact can be identified, and the tilted rectangle of the stationary contact can be identified by using the adaptive rotating template matching algorithm proposed in this paper. The coordinates of the two upper vertices of the rectangle are obtained as (x_1,y_1) and (x_2,y_2), respectively.

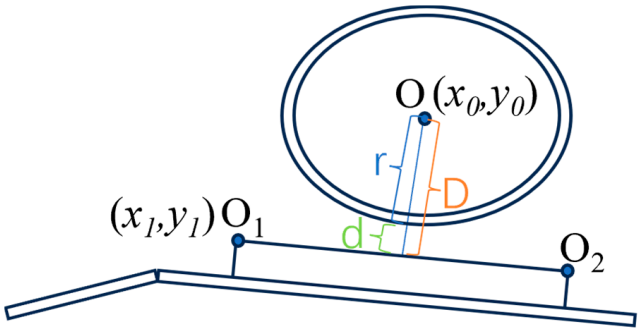

Figure 12. Diagram for judging the contact status of the moving contact and the stationary contact.

The expression of the line on which the upper edge of the rectangle lies is first computed from the coordinates of the vertices of the rectangle, and the equation of the line is represented by the two-point formula:

$$\frac{(y-y_1)}{(x-x_1)} = \frac{(y_2-y_1)}{(x_2-x_1)} \tag{20}$$

Summarizing after collation yields the general form equation as follows:

$$(y_2-y_1)x-(x_2-x_1)y+(y_1x_2-y_2x_1)=0 \tag{21}$$

In the general form equation, the equation is simplified for subsequent calculations by applying the following:

$$\begin{cases} A = y_2 - y_1 \\ B = -(x_2 - x_1) \\ C = y_1 x_2 - y_2 x_1 \end{cases} \tag{22}$$

Therefore, the straight line can be simplified as follows:

$$Ax + By + C = 0 \tag{23}$$

From this, the vertical distance from the center of the circle of the moving contact to the upper edge of the stationary contact can be calculated as follows:

$$D = \frac{|Ax_0 + By_0 + C|}{\sqrt{A^2 + B^2}} \tag{24}$$

By subtracting the radius of the moving contact from this distance, the vertical distance between the moving contact and the stationary contact can be calculated as follows:

$$\mathrm{d} = D - r = \frac{|Ax_0 + By_0 + C|}{\sqrt{A^2 + B^2}} - r \tag{25}$$

Assuming that the distance from the center of the circle of the moving contact to the stationary contact in the i-th frame image is d_i, it is only necessary to determine whether this distance is greater than the radius of the moving contact, i.e., whether the distance between the moving contact and the stationary contact is zero, to determine the contact state of the moving contact and the stationary contact in the image, and the formula is expressed as follows:

$$\begin{cases} d_{\mathrm{i}} > 0 & \text{the moving contact in contact with the stationary contact} \\ d_{\mathrm{i}} = 0 & \text{no contact between the moving contact and the stationary contact} \end{cases} \tag{26}$$

A relay was selected for testing, and some of the test data during the contact of the moving contact and the stationary contact are shown in Table 4, where the data were taken at intervals of five frames of images.

Table 4. Partial test data during contact.

Time/s	r/mm	D/mm	d/mm
1.65	4.56	4.56	0
1.6505	4.56	4.56	0
...	...	...	...
1.6665	4.56	4.56	0
1.667	4.56	4.58881	0.02881
1.6675	4.56	4.59472	0.03472
1.668	4.56	4.6025	0.0425
1.6685	4.56	4.62249	0.06249
1.669	4.56	4.63165	0.07165
1.6695	4.56	4.63535	0.07535
1.67	4.56	4.6401	0.0801
1.6705	4.56	4.64356	0.08356
1.671	4.56	4.64636	0.08636
1.6715	4.56	4.64856	0.08856
1.672	4.56	4.64889	0.08889
1.6725	4.56	4.64473	0.08473
1.673	4.56	4.63865	0.07865
1.6735	4.56	4.63238	0.07238
1.674	4.56	4.62678	0.06678

Table 4. *Cont.*

Time/s	r/mm	D/mm	d/mm
1.6745	4.56	4.61795	0.05795
1.675	4.56	4.60524	0.04524
1.6755	4.56	4.59257	0.03257
1.676	4.56	4.58526	0.02526
1.6765	4.56	4.56	0
...	...	...	...
1.6995	4.56	4.56	0
1.7	4.56	4.56	0

The bounce distance of the contacts is the distance between the moving contact and the stationary contact after the occurrence of a bounce. To provide a clearer observation of the relay contact bounce, the bounce distance is plotted and displayed in Figure 13.

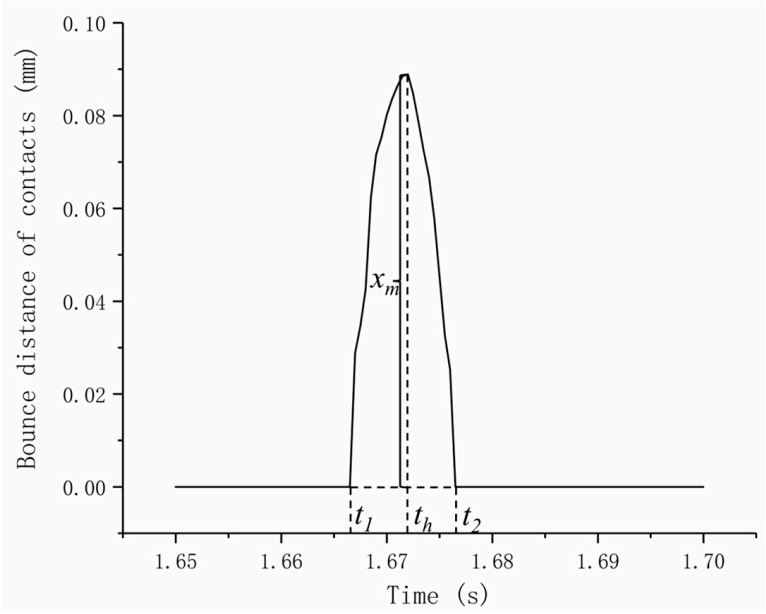

Figure 13. Curve of change in distance between moving contact and stationary contact during contact bounce.

The analysis of the data and curves reveals that the relay experiences a contact bounce during the action process. Specifically, at t_1 = 1.667 s, the moving contact and the stationary contact separate, and at t_2 = 1.676 s, they restore contact and continue to maintain the contact state. Therefore, the calculation of the contact bounce time for this group is obtained as follows:

$$t_{ht} = t_2 - t_1 = 1.676 - 1.667 = 0.009 \text{ s} = 9 \text{ ms} \quad (27)$$

During the contact bounce process, the maximum bounce distance, x_m, between the moving contact and the stationary contact represents the bounce height, h, of the contacts. Therefore, the bounce height of the contacts is as follows:

$$h = x_m = d_{max} = 0.0889 \text{ mm} \quad (28)$$

The time, t_m, required for the contacts to bounce to the maximum distance can be obtained by analyzing the data:

$$t_m = t_h - t_1 = 1.672 - 1.667 = 0.005 \text{ s} = 5 \text{ ms} \quad (29)$$

where t_h represents the moment when the moving contact and the stationary contact bounce to the maximum distance.

The above analysis demonstrates that examining contact bounce through high-speed shooting and image processing enables the calculation of not only the relay's contact bounce time but also the contact bounce height and the time required for the contact to bounce to the maximum distance. This allows for a more comprehensive analysis of the entire contact bounce process.

4.2. Analysis of Contact Bounce Causes

To obtain a better understanding of the timing and status of contact bounce, the moving contact in the image is subjected to Hough circle detection. Subsequently, the detected moving contact is tracked using the KCF (Kernel Correlation Filter) algorithm for target tracking, resulting in the displacement curve of the moving contact along the y-axis. Next, the displacement curve of the moving contact along the y-axis is merged with the corresponding displacement curve of the contact bounce distance over time. The results, depicted in Figure 14, indicate that contact bounce occurs at the highest point of the first upward displacement during the joint vibration of the moving contact and the stationary contact following the relay's release.

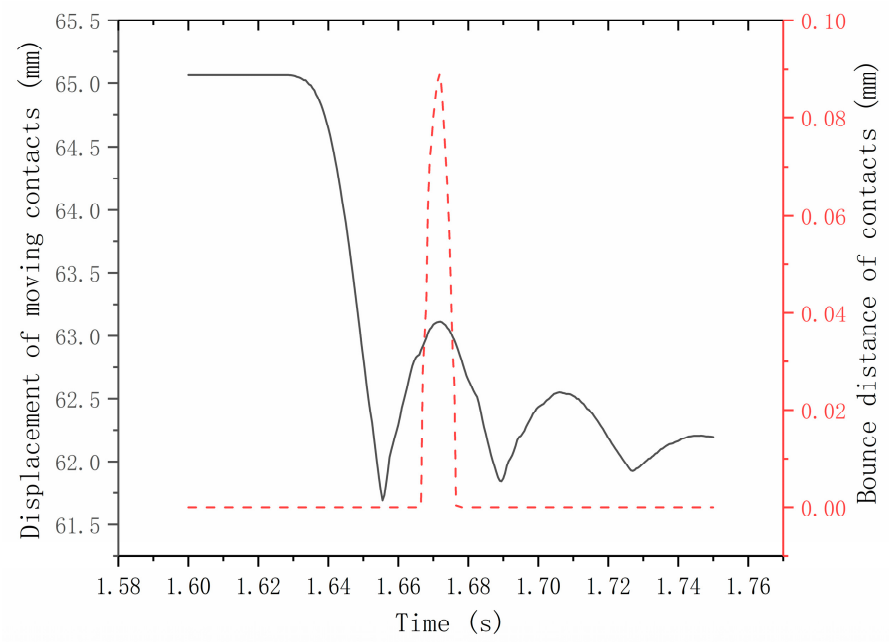

Figure 14. Curve of distance between contacts and displacement of moving contacts during contact bounce.

Considering the structure of the relay and the displacement curve of the moving contact, let us analyze the reasons for the observed phenomenon: In the relay studied in this paper, the reed for the stationary contact has a certain elasticity. Therefore, the stationary contact does not remain fixed after coming into contact with the moving contact; instead, it undergoes some elastic deformation due to the continued movement of the moving contact. This results in the stationary contact moving in tandem with the moving contact, experiencing mutual vibration. Consequently, contact bounce does not immediately occur after the contact of the moving and stationary contacts, significantly reducing the likelihood of contact bounce in the relay.

However, there are still instances of contact bounce in some relays. This is attributed to the fact that during the mutual vibration process after the contact between the moving contact and the stationary contact, the kinetic energy of the contacts is significant. Due to the presence of the brackets, the upward movement of the reed for the stationary contact is

restricted. As a result, when the stationary contact reaches the highest point of vibration, the kinetic energy of the moving contact is not zero. It continues to move upward for a certain distance, leading to the separation of the moving and stationary contacts and causing contact bounce. Furthermore, the occurrence of this phenomenon is closely related to the elasticity of the contact spring. The greater the elasticity of the spring, the higher the contact can bounce after contact, making it more likely to be restricted by the retainer and leading to contact separation.

Based on the above research results, it is evident that relay contact bounce mainly occurs during the vibration process of the contact. In practical applications, this issue can be mitigated by altering the material or structure of the relay contact spring to reduce its elasticity, thereby reducing the amplitude of contact vibration and suppressing contact bounce. Alternatively, adjusting the position of the retainer appropriately can prevent it from restricting the maximum height of the stationary contact spring during its rebound, thus avoiding the separation of the moving contact from the stationary contact during vibration and preventing contact bounce.

5. Conclusions

This paper captured images of the relay contact motion process through high-speed filming. Addressing the situation where the angle of the stationary contact continuously changes, a rotation template matching algorithm based on adaptive weight is proposed for the identification of the stationary contact. The analysis of the identified stationary contact is used to explore the phenomenon of relay contact bounce, leading to the following conclusions:

(1) The adaptive weight rotation template matching algorithm proposed in this paper achieves accurate recognition and matching for changes in target angles, enabling the retrieval of target rotation angles. It can be applied to scenarios where targets continuously rotate in images. However, the algorithm is still sensitive to changes in the scale of the target. Additionally, there is considerable room for improvement in recognition speed, particularly when high precision is required. Therefore, future work should focus on refining and optimizing the algorithm to address these challenges.

(2) Image analysis allows for the assessment of the contact status, enabling the analysis of the relay contact bounce process. Parameters such as the contact bounce time, the bounce height, and the time required for the contact to open to the bounce height are calculated. Additionally, a curve depicting the contact bounce distance is generated.

(3) The analysis of the motion curve of the relay contact during the contact bounce process reveals that contact bounce in the studied relay occurs at the highest point of upward vibration after the contact between the moving and stationary contacts. The identified cause is the limitation imposed by the brackets on the upward movement of the reed for the stationary contact when the kinetic energy of the contact is significant, leading to the separation of the moving and stationary contacts. This discovery provides a basis for improving the relay's structural design.

Author Contributions: Conceptualization, W.L. and W.Z.; methodology, X.W.; software, W.Z. and J.Y.; validation, X.W., J.Y. and W.W.; formal analysis, W.Z., J.Y. and X.Y.; investigation, W.Z. and J.Y.; resources, X.W.; data curation, W.W.; writing—original draft, W.Z.; writing—review and editing, W.L.; visualization, X.Y.; supervision, W.L.; project administration, W.Z.; funding acquisition, W.L. All authors have read and agreed to the published version of the manuscript.

Funding: This research was funded by the Innovative Research Group Program of the Natural Science Foundation of Hebei Province, grant number E2020202142.

Institutional Review Board Statement: Not applicable.

Informed Consent Statement: Not applicable.

Data Availability Statement: The data presented in this study are available upon request from the corresponding author due to confidentiality restrictions.

Conflicts of Interest: Author Xin Wang was employed by the company Shenyang Railway Signal Co., Ltd. The remaining authors declare that the research was conducted in the absence of any commercial or financial relationships that could be construed as a potential conflict of interest.

References

1. Zhai, G.F.; Cui, X.L.; Yang, W.Y. Overview of electromagnetic relay products and research technology development. *Electr. Appl. Energy Effic. Manag. Technol.* **2016**, 1–8. [CrossRef]
2. Mcbride, J.W. An experimental investigation of contact bounce in medium duty contacts. *IEEE Trans. Compon. Hybrids Manuf. Technol.* **1991**, *14*, 319–326. [CrossRef]
3. Slonim, A. Bouncing of Contacts under Current Load (The Influence of Mechanical System Parameters and Load Current on the Closing Process of Electrical Contacts). *IEEE Trans. Compon. Hybrids Manuf. Technol.* **1987**, *10*, 122–126. [CrossRef]
4. Mcbride, J.W. Electrical contact bounce in medium-duty contacts. *IEEE Trans. Compon. Hybrids Manuf. Technol.* **1989**, *12*, 82–90. [CrossRef]
5. Miedzinski, B.; Kristiansen, M. Analytical and experimental investigations of reed contact bouncing. *IEEE Trans. Compon. Hybrids Manuf. Technol.* **1988**, *11*, 200–210. [CrossRef]
6. Liu, L.X.; Yang, W.Y.; Chen, Z.; Zhai, G.F.; Zio, E. A Novel Nonlinear Dynamic Model for Predicting Contact Bounce of Electromagnetic Relays with Flexible Spring Components. *IEEE Trans. Compon. Packag. Manuf. Technol.* **2022**, *12*, 1318–1328. [CrossRef]
7. Liu, L.X.; Chen, Z.; Yang, W.Y.; Zhai, G.F.; Zio, E.; Kang, R. A novel methodology for the optimization of design parameters of electromagnetic relays. *Nonlinear Dyn.* **2023**, *112*, 2909–2932. [CrossRef]
8. Liu, L.X.; Yang, W.Y.; Chai, Y.Y.; Zhai, G.F. Rigid-flexible coupling collision dynamics modeling method and bouncing behavior analysis of microminiature relays. *Chin. J. Electr. Eng.* **2022**, *42*, 808–818.
9. Yang, W.Y.; Liu, L.X.; Liu, Y.; Zhai, G.F. Modeling of contactor dynamics considering collision bouncing and analysis of factors influencing its bouncing characteristics. *J. Electrotechnol.* **2019**, *34*, 1900–1911.
10. Yang, C.N.; Zheng, Z.; Ren, W.B. Investigation of making process and associated contact bounce behaviors for alternating current contactor. In Proceedings of the IEEE Sixty-Sixth Holm Conference on Electrical Contacts (HLM), San Antonio, TX, USA, 24–27 October 2021; pp. 165–170.
11. Ren, W.B.; Jiang, N.; Chang, C.; Xue, S.J.; Chen, Y.; Coutu, R.A. Observation and Understanding of the Initial Unstable Electrical Contact Behaviors. *IEEE Trans. Compon. Packag. Manuf. Technol.* **2017**, *7*, 1272–1279. [CrossRef]
12. Ren, W.B.; He, Y.; Jin, J.B.; Man, S.D. Investigations of the contact bounce behaviors and relative dynamic welding phenomena for electromechanical relay. *Rev. Sci. Instrum.* **2016**, *87*, 065111. [CrossRef]
13. Tang, Z.; Xu, Z. Optimal Design Method for AC Contactor Spring System Based on Response Surface Method. *Trans. China Electrotech. Soc.* **2022**, *37*, 515–527.
14. Wang, Y.; Xu, Z. RBR Control Strategy for the Closing Process of Intelligent Electromagnetic Contactor. *Proc. Chin. Soc. Electr. Eng.* **2019**, *39*, 4568–4578.
15. Wu, J.; Xu, Z. A Model-free Adaptive Control Strategy for Actuation of Electromagnetic Contactors. *Proc. Chin. Soc. Electr. Eng.* **2020**, *40*, 1663–1673.
16. Huang, K.; Wang, F.; Zhao, M.; Guo, B.; Ou, D. Vibration Characteristic Analysis Based on Contact Bounce of Contactor. *J. Vib. Meas. Diagn.* **2022**, *42*, 1177–1183.
17. Huang, K.; Wang, F.; Zhao, M.; Li, Y.; Ou, D. Analysis and algorithm optimization of contact bounce behavior of contactors. *J. Chongqing Univ.* **2021**, *44*, 103–113.
18. Li, Z.; Wang, F.Z.; Huang, K.P.; Li, W.X. Analysis and parameter optimization of contact bounce of vacuum circuit breaker. *J. Meas. Sci. Instrum.* **2023**, *14*, 226–232.
19. Winkel, F.; Scholz, P.; Wallscheid, O.; Böcker, J. Reducing Contact Bouncing of a Relay by Optimizing the Switch Signal During Run-Time. *IEEE Trans. Autom. Sci. Eng.* **2023**, 1–11. [CrossRef]
20. Chen, H.; Hu, X.; Fu, R.; Wang, R.; Liang, H.; Yu, H. Polarized Relay Contact Gap Measurement Based on Machine Vision Technology. In Proceedings of the 6th International Conference on Instrumentation & Measurement, Computer, Communication and Control (IMCCC 2016), Harbin, China, 21–23 July 2016; pp. 623–628.
21. Sun, T.-H.; Tseng, C.-C.; Chen, M.-S. Electric contacts inspection using machine vision. *Image Vis. Comput.* **2010**, *28*, 890–901. [CrossRef]
22. Cao, Q.H.; Liu, X.J. Simulation analysis and experimental research on arc motion of high-voltage DC relays. *J. Electr. Eng. Technol.* **2019**, *34*, 4699–4707.
23. Lu, J.G.; Zhang, N.K.; Wang, J.Q. Study of relay contact bounce. *J. Electrotechnol.* **1988**, 6–12. [CrossRef]
24. Attak, S.; Wu, A.; Claeys, J.P.; Sannino, L.; Meley, J.P.; Papillon, A.; Bonjean, E.; Ferrazzi, M.; Godechot, X. Medium Voltage Vacuum Circuit Breakers Boucing Time Overall Study. In Proceedings of the 30th International Symposium on Discharges and Electrical Insulation in Vacuum (ISDEIV), Okinawa, Japan, 25–30 June 2023; pp. 445–448.

25. Fang, Y.Q.; Ren, W.B. Experimental study on the phenomenon of contact closure bounce of electromagnetic relay. *Electr. Appl. Energy Effic. Manag. Technol.* **2020**, 5–9. [CrossRef]
26. Huo, G.; Lu, J.; Luo, S. Image Stitching Based on CLAHE and Improved ZNCC. *Laser Optoelectron. Prog.* **2022**, *59*, 226–234.